

Measurement-Induced Spectral Transition

Ken Mochizuki^{1,2} and Ryusuke Hamazaki^{2,3}

¹*Department of Applied Physics, University of Tokyo, Tokyo 113-8656, Japan*

²*Nonequilibrium Quantum Statistical Mechanics RIKEN Hakubi Research Team,*

RIKEN Cluster for Pioneering Research (CPR), 2-1 Hirosawa, Wako 351-0198, Saitama, Japan

³*RIKEN Interdisciplinary Theoretical and Mathematical Sciences*

Program (iTHEMS), 2-1 Hirosawa, Wako 351-0198, Saitama, Japan

We show that noisy quantum dynamics exposed to weak measurements exhibit a spectral transition between gapless and gapped phases. To this end, we employ the Lyapunov spectrum obtained through singular values of a non-unitary matrix describing the dynamics. We discover that the gapless and gapped phases respectively correspond to the volume-law and area-law phases of the entanglement entropy for the dominant Lyapunov vector. This correspondence between the spectral gap and the scaling of entanglement offers an intriguing analogy with ground-state phase transitions. We also discuss some crucial differences from ground-state transitions, such as the scaling law of the entanglement and the exponentially small gaps. Furthermore, we show that the spectral transition leads to the transition of the timescale for the memory loss of initial states.

Introduction.— In a quantum system described by a time-independent generator, such as the Hamiltonian for isolated systems and the Liouvillian for dissipative systems, the generator’s spectrum and gap provide essential information about the system. For example, quantum phase transitions of ground states are accompanied by the gap closing of the Hamiltonian [1, 2], and the Liouvillian gap is related to the asymptotic decay rate towards the stationary state [3–9]. For the quantum phase transitions, ground states in gapless regimes exhibit behaviors qualitatively different from those in gapped phases in terms of the entanglement entropy and correlation functions [10–13].

The entanglement entropy, which captures intrinsic features of quantum states, has also attracted recent huge attention in noisy dynamics of monitored quantum systems, where generators depend on time randomly. Owing to the competition between unitary dynamics and quantum measurements, where the former and latter respectively enhance and suppress the entanglement growth, measurement-induced entanglement transitions occur [14–42]. Many intriguing aspects of such measurement-induced transitions have been explored, including critical properties [14, 17, 18, 21, 23, 25, 34, 41, 42], timescales of relaxation [22, 28, 29, 38, 43], and multifractality [33].

Then, a natural question is whether the measurement-induced phase transitions under noisy dynamics can be understood as a spectral transition as for the ground-state phase transition in equilibrium. Unfortunately, this problem has been elusive due to the intrinsic randomness in the quantum measurement process.

In this Letter, we discover a measurement-induced spectral transition leading to the entanglement transition, in analogy with the ground-state phase transitions between gapless and gapped phases. While our monitored system lacks a time-independent generator, we here focus on the Lyapunov spectrum

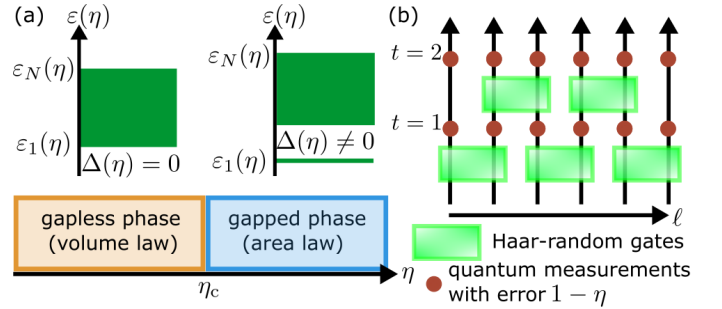


FIG. 1. (a) Schematic figure of the spectral transition. With varying a parameter η , the transition occurs between the gapless and gapped phases, where $\{\varepsilon_i(\eta)\}$ are the Lyapunov spectra of the time-evolution matrix. The transition point of the spectral transition coincides with that of the entanglement transition between the volume-law and area-law phases for the dominant Lyapunov vector corresponding to $\varepsilon_1(\eta)$. (b) Our model for the dynamics of qubits under measurements. After local unitary gates are applied, quantum measurements with errors $1 - \eta$ are carried out for all sites.

obtained through singular values of a random non-unitary matrix describing the dynamics. As a result, we find a spectral transition from the gapless phase to the gapped phase, as shown in Fig. 1 (a). The gapless and gapped phases respectively correspond to the volume-law and area-law phases of the entanglement entropy for the dominant Lyapunov vector after long times. Such correspondence between the entanglement scaling and the spectral gap is similar to the entanglement transitions of ground states [10–13]. Meanwhile, in gapless phases, we find that the volume-law of entanglement entropy and exponentially small spectral gaps of monitored dynamics are distinct from the logarithmic-law of entanglement entropy and polynomially small spectral gaps of ground states. We further argue that the spectral transition leads to the transition of the timescale at

which observables become independent of initial states, reminiscent of the purification transition.

Setup.— We consider quantum dynamics depicted in Fig. 1 (b), where L qubits are arrayed on a one-dimensional chain. The local unitary gates, which generate entanglement between nearest neighbor qubits, are given by 4×4 Haar-random unitary matrices. These gates are arranged in a brick-wall manner under the open boundary condition, where the unitary matrix at each time t is denoted as U_t . The weak quantum measurements at time t , described by Kraus operators $M_t(\eta) = \bigotimes_{\ell=1}^L M_{\omega_{t,\ell}}(\eta)$ with

$$M_{\pm}(\eta) = \frac{\sigma_0 \pm \eta \sigma_3}{\sqrt{2(1 + \eta^2)}}, \quad (1)$$

include the error $1 - \eta$ where $0 \leq \eta \leq 1$. Here, σ_0 is the 2×2 identity matrix, σ_3 is the z component of the Pauli matrices, ℓ represents a position of a qubit, and $\omega_{t,\ell}$ takes $+$ or $-$, which correspond to the measurement outcomes for σ_3^{ℓ} under the error with σ_3^{ℓ} being the Pauli matrix at ℓ . The probability distribution of $\{\omega_{t,\ell}\}$ is determined through the Born rule. The parameter η describes the strength of the measurement, where $\eta = 1$ and $\eta = 0$ correspond to the projective measurement and no measurement, respectively. The dynamics from an initial pure state $|\psi_0\rangle$ becomes $|\psi_t(\eta)\rangle = V_t(\eta)|\psi_0\rangle / \sqrt{\langle\psi_0|V_t^\dagger(\eta)V_t(\eta)|\psi_0\rangle}$, where $V_t(\eta) = M_t(\eta)U_tM_{t-1}(\eta)U_{t-1}\cdots M_1(\eta)U_1$ implicitly depends on measurement outcomes $\{\omega_{t,\ell}\}$.

We define an effective ‘‘Hamiltonian,’’

$$K_t(\eta) = -\frac{1}{2t} \ln \left[V_t(\eta)V_t^\dagger(\eta) \right], \quad (2)$$

which leads to an analogy between ground-state phase transitions and measurement-induced transitions. The eigenvalues of $K_t(\eta)$, $\{\varepsilon_{t,i}(\eta, L)\}$, are arrayed as $\varepsilon_{t,i}(\eta, L) \leq \varepsilon_{t,i+1}(\eta, L)$ with $1 \leq i \leq N := 2^L$, where the singular values of $V_t(\eta)$ become $\Lambda_{t,i}(\eta) = e^{-\varepsilon_{t,i}(\eta)t}$. The i th Lyapunov vector $|\Psi_{t,i}(\eta)\rangle$ is the eigenmode of $K_t(\eta)$ whose eigenvalue is $\varepsilon_{t,i}(\eta)$. The dominant Lyapunov vector $|\Psi_{t,1}(\eta)\rangle$ corresponds to the ground state of the effective Hamiltonian.

As an indicator for the measurement-induced phase transition, we focus on the spectral gap,

$$\Delta(\eta, L) = \varepsilon_2(\eta, L) - \varepsilon_1(\eta, L), \quad (3)$$

where $\varepsilon_i(\eta) = \lim_{t \rightarrow \infty} \varepsilon_{t,i}(\eta)$. When t is sufficiently large such that $\Delta_t(\eta, L) = \varepsilon_{t,2}(\eta, L) - \varepsilon_{t,1}(\eta, L) \simeq \Delta(\eta, L)$, the spectral gap $\Delta(\eta, L)$ gives the relaxation time

$$\tau_\delta(\eta, L) = \left\lfloor \frac{\ln(\delta)}{\Delta(\eta, L)} \right\rfloor, \quad (4)$$

at which $|\Psi_{t,i}(\eta)\rangle$ with $i \geq 2$ become negligible within the precision δ and thus $|\psi_t(\eta)\rangle \simeq |\Psi_{t,1}(\eta)\rangle$ is realized. The

dominant Lyapunov vector is similar to the stationary states in open quantum systems described by static generators, in the sense that they are realized in the long-time regime irrespective of initial states. On the other hand, they exhibit distinct behaviors; $|\Psi_{t,1}(\eta)\rangle$ randomly fluctuates in time, while stationary states are independent of time.

We note that, in several settings, the spectral gap has been computed at the transition point to extract critical properties of measurement-induced transitions [34, 41, 42]. In contrast, we explore the scaling of $\Delta(\eta, L)$ and eigenstate properties in a wide parameter region of η .

Transition of the spectral gap.— Our monitored dynamics exhibit a transition in terms of the Lyapunov spectrum. Figure 2 (a) shows spectral gaps $\Delta(\eta, L)$ for various η and L . The details of the numerical calculations are given in Supplemental Material [44]. We can understand that $\Delta(\eta, L)$ rapidly decreases with increasing L for small η , which indicates $\Delta(\eta) = 0$, where

$$\Delta(\eta) = \lim_{L \rightarrow \infty} \Delta(\eta, L). \quad (5)$$

In contrast, $\Delta(\eta, L)$ is almost independent of L for large η , which indicates $\Delta(\eta) \neq 0$. To compute $\Delta(\eta)$, we extrapolate $\Delta(\eta, L)$ using the fitting function $\Delta_{\text{fit}}(\eta, L) = \Delta(\eta) + \alpha(\eta)[\beta(\eta)]^{-L}$. Through the least-square fitting with $10 \leq L \leq 22$, we obtain Fig. 2 (b), which clearly shows the transition between the gapless phase with $\Delta(\eta) = 0$ and the gapped phase with $\Delta(\eta) \neq 0$. Indeed, for $\eta < \eta_c = 0.2$ ($\eta \geq \eta_c$), we see that the bottom value of the error bar is smaller (larger) than 0, indicating that the system is in the gapless (gapped) phase. The spectral transition originates from the competition between unitary dynamics and quantum measurements since the transition vanishes when there is no unitary gate [44]. We note that Refs. [45, 46] explore Lyapunov exponents and purification times of dynamics evolved by non-local matrices, where no transition is found. This indicates that the locality of U_t and $M_t(\eta)$ plays a key role in measurement-induced transitions, which is also pointed out in Refs. [30, 31].

Ground states in isolated quantum systems also exhibit the gapless-gapped transition, and the behaviors of the gaps in isolated systems and our monitored dynamics are qualitatively similar in gapped phases, as written in Table I. Meanwhile, there is a qualitative difference in gapless phases; our monitored dynamics exhibit $\Delta(\eta, L) \propto \exp[-L/\xi(\eta)]$ with $\xi(\eta) = 1/\ln[\beta(\eta)]$, in contrast to spectral gaps of local Hamiltonians in the critical phase obeying $1/\text{poly}(L)$ [47].

Transition of the entanglement.— We show that the above spectral transition corresponds to the entanglement transition. We present the entanglement transition for the dominant Lyapunov vector $|\Psi_{t,1}(\eta)\rangle$ to make a clear comparison with ground-state phase transitions. Note that the correspondence also applies

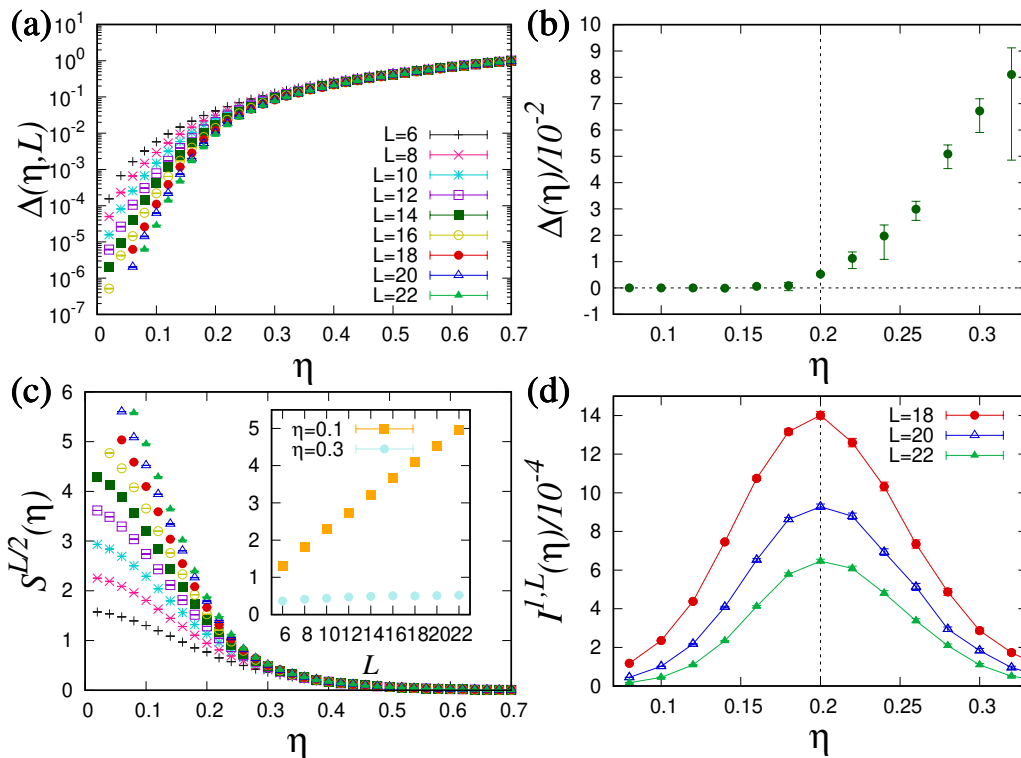


FIG. 2. (a) The spectral gap $\Delta(\eta, L)$ as functions of η for various system sizes L . $\Delta(\eta, L)$ rapidly decreases with increasing L for small η , while it is almost constant for large η . (b) The spectral gap $\Delta(\eta)$ in the thermodynamic limit. The spectral transition between the gapless and gapped phases occurs around $\eta_c = 0.2$. (c) The entanglement entropy $S^{L/2}(\eta)$ of the dominant Lyapunov vector $|\Psi_{t,1}(\eta)\rangle$ for various error parameters η and system sizes L . The inset shows $S^{L/2}(\eta)$ as functions of the system size L , where the gapless and gapped phases exhibit the volume-law (orange squares) and the area-law (blue circles) scalings of $S^{L/2}(\eta)$. (d) The mutual information averaged over $T = 10^5$ steps after $\tau \geq \tau_\delta(\eta, L)$. There is a peak around η_c , corresponding to the entanglement transition between the volume-law and area-law phases. The thresholds of the spectral transition and the entanglement transition coincide.

	ground-state transition in equilibrium	measurement-induced transition in noisy dynamics
gapped phase	gap: $O(L^0)$, entanglement entropy: $O(L^0)$	gap: $O(L^0)$, entanglement entropy: $O(L^0)$
gapless phase	gap: $O[1/\text{poly}(L)]$, entanglement entropy: $O[\ln(L)]$	gap: $O(e^{-L})$, entanglement entropy: $O(L)$

TABLE I. Comparison between ground-state transitions in one-dimensional isolated quantum systems and the measurement-induced transition explored in this work, in terms of the spectral gap and the half-chain entanglement entropy. Behaviors in gapped phases are qualitatively similar, while those in gapless phases are distinct.

to the entanglement transition for states after $t \propto L$, often discussed in previous works [18], while the data is not shown.

We show that the threshold around $\eta_c = 0.2$ of the spectral transition corresponds to that of the entanglement entropy for $|\Psi_{t,1}(\eta)\rangle$. To this end, we compute the entanglement entropy averaged over $T = 10^4$ time steps after $\tau \geq \tau_\delta(\eta, L)$ with $\delta = 10^{-2}$, $S^A(\eta) = \frac{1}{T} \sum_{t=\tau+1}^{\tau+T} S_t^A(\eta)$, where $S_t^A(\eta) = -\text{tr}_A(\rho_t^A(\eta) \ln[\rho_t^A(\eta)])$ with $\rho_t^A(\eta) = \text{tr}_{\bar{A}}(|\psi_t(\eta)\rangle \langle \psi_t(\eta)|)$. Here, $\text{tr}_{\bar{A}}$ is the partial trace with respect to the complement of the subsystem A . Figure 2 (c) shows the entanglement entropy as functions of η for various L . We can see that

the entanglement entropy of the half chain exhibits the volume-law scaling, $S^{L/2}(\eta) \propto L$, for small η . On the other hand, the entanglement entropy exhibits the area-law scaling for large η , $S^{L/2}(\eta) \propto L^0$.

It is known that the transition point between the volume-law and area-law phases exhibits the peak of the mutual information $I_t^{A,B}(\eta) = S_t^A(\eta) + S_t^B(\eta) - S_t^{A,B}(\eta)$ for $|\psi_t(\eta)\rangle$ [17]. Figure 2 (d) shows the mutual information of $|\psi_t(\eta)\rangle \simeq |\Psi_{t,1}(\eta)\rangle$ averaged over $T = 10^5$ time steps, $I^{1,L}(\eta) = \frac{1}{T} \sum_{t=\tau+1}^{\tau+T} I_t^{A,B}(\eta)$, where A and B are qubits at $\ell = 1$ and $\ell = L$, respectively. We can see that $I^{1,L}(\eta)$ exhibits a peak around $\eta_c = 0.2$, which coincides with the spectral transition. We note that a

peak of the mutual information is also reported in Ref. [17] while the boundary condition differs from that in the present work.

The coincidence between thresholds of the spectral transition and the entanglement transition is analogous to ground-state phase transitions between gapless and gapped phases in equilibrium [10–13]. In particular, behaviors of the entanglement entropy in gapped phases are qualitatively similar, as listed in Table I. This suggests that the relation between the spectral gap and the scaling of the entanglement also applies to non-equilibrium phenomena, as well as the equilibrium physics. Meanwhile, $|\Psi_{t,1}(\eta)\rangle$ of the gapless monitored dynamics with $\eta < \eta_c$ and the ground states of gapless Hamiltonians have a crucial difference; the entanglement exhibits the volume-law scaling in the former case and the logarithmic scaling in the latter case [48]. We note that gapless phases in equilibrium exhibit criticality, while critical behaviors of measurement-induced transitions are observed at the transition point [14, 17, 18, 21, 23, 25, 34, 41, 42], which may be the key to understand the distinction in gapless phases.

Memory loss effect.— The spectral transition also leads to the transition of the timescale for the memory loss, i.e., $\tau_\delta(\eta, L) \simeq O(e^L)$ in the gapless phase and $\tau_\delta(\eta, L) \simeq O(L^0)$ in the gapped phase. Indeed, if we fix $V_t(\eta)$, $|\psi_t(\eta)\rangle \simeq |\Psi_{t,1}(\eta)\rangle$ is independent of initial states $|\psi_0\rangle$ for $t \geq \tau_\delta(\eta, L)$ within the precision δ . Figure 3 shows $\langle \psi_t(\eta) | X | \psi_t(\eta) \rangle$ with $X = \sum_\ell \sigma_1^\ell$ for several trajectories starting from different initial states, where $\sigma_1^\ell = \left(\bigotimes_{m=1}^{\ell-1} \sigma_0\right) \otimes \sigma_1 \otimes \left(\bigotimes_{m=\ell+1}^L \sigma_0\right)$ is the x component of the Pauli matrices at the site ℓ . Here, $V_t(\eta)$ is generated through the Born rule based on one trajectory, and the same $V_t(\eta)$ is also applied to the other initial states. We can see that the expectation values corresponding to different initial states take almost the same value when $t \geq \tau_\delta(\eta, L)$ with $\delta = 10^{-2}$, while different initial states lead to different expectation values when $t \ll \tau_\delta(\eta, L)$. We can understand that the timescale $\tau_\delta(\eta, L)$ of the memory loss effect for $\eta < \eta_c$ is much larger than that for $\eta > \eta_c$, due to the spectral transition.

We conjecture that the spectral gap, which becomes independent of trajectories in our monitored dynamics of pure states [44], takes the same value even when the initial state is a mixed state. This conjecture means that the spectral transition and thus the entanglement transition in the weakly monitored dynamics correspond to the purification transition: the volume-law (area-law) phase exhibits an exponentially long (constant) timescale in the system size for the initial mixed state to become a pure state approximately. This is consistent with the purification transition exposed to projective measurements [22], while the relation with the spectral transition has never been discussed before.

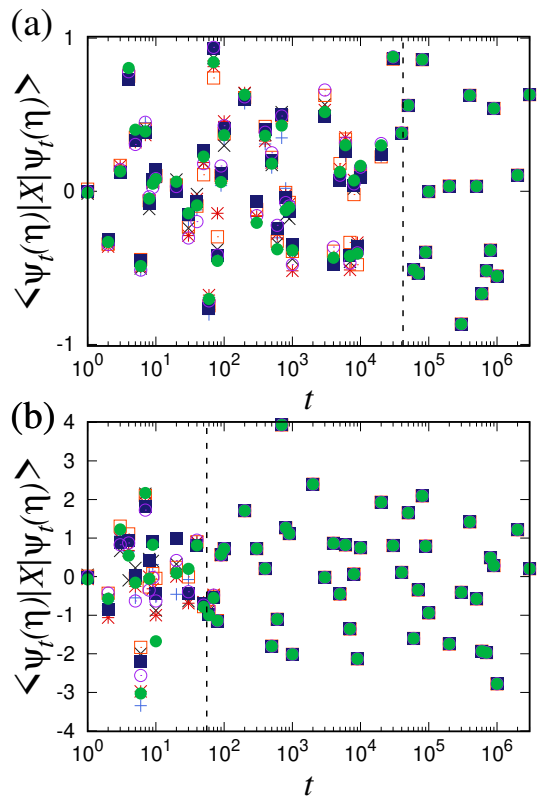


FIG. 3. Expectation values of $X = \sum_\ell \sigma_1^\ell$ with (a) $\eta = 0.1$ in the gapless phase and (b) $\eta = 0.3$ in the gapped phase. The black broken lines represent $\tau_\delta(\eta, L) = |\ln(\delta)/\Delta(\eta, L)|$ with $\delta = 10^{-2}$. Here, different symbols correspond to randomly chosen different initial states, and the same $V_t(\eta)$ is applied to all initial states. The expectation values become almost the same after $\tau_\delta(\eta, L)$, and the timescale in the gapless phase is much longer than that in the gapped phase. The system size is $L = 18$ in both (a) and (b).

Structures of the entire spectrum.— While we have focused on the spectral gap, we next compare the entire spectrum of the monitored dynamics with that of Hamiltonians in one-dimensional systems. Spectra of locally interacting many-body Hamiltonians usually have the following two structures: (a) the width of the spectrum becomes $O(L)$, which means that the typical level spacing is $O(e^{-L})$, and (b) the spectral gap becomes $O[1/\text{poly}(L)]$ in gapless regimes or constant above a few states exponentially close to the ground state in gapped phases. We can analytically show that $\{\varepsilon_i(\eta)\}$ of our monitored dynamics also satisfy (a). Indeed, employing the majorization, the Horn theorem, and properties of doubly stochastic matrices [49], we can obtain [44]

$$\varepsilon_N(\eta, L) - \varepsilon_1(\eta, L) \leq L \ln \left(\frac{1+\eta}{1-\eta} \right). \quad (6)$$

On the other hand, the monitored dynamics do not satisfy (b) in the gapless phase; the Lyapunov spectra

of low-lying excited states become $O(e^{-L})$, which is numerically illustrated in Supplemental Material [44].

Discussion.— We have shown that the quantum dynamics exposed to weak measurements exhibit the spectral transition in terms of the Lyapunov spectrum, whose transition point coincides with that of the entanglement transition. This coincidence is analogous to ground-state phase transitions between gapless and gapped phases, while the scalings of the entanglement and the gap in the monitored dynamics are qualitatively different from those in isolated quantum systems. To establish the analogy and clarify the distinction between these transitions, exploring the locality of $K_t(\eta)$ should be an important future direction. While ground states in condensed matter models are usually determined from local Hamiltonians, it is non-trivial whether $K_t(\eta)$ becomes local. This distinction may be the origin of the difference in the scalings of the spectral gap and entanglement in gapless phases of these two transitions.

We have also shown that the spectral transition corresponds to the transition of the timescale for the memory loss of a pure state and conjectured that it also corresponds to the purification transition of mixed states. In monitored dynamics with projective measurements, where the purification transition is also reported [22], singular values of time-evolution operators can be strictly zero, and the Lyapunov spectrum with $i > 1$ become ill-defined when the projective measurement is done to all qubits. In contrast, singular values $\{\Lambda_{t,i}(\eta)\}$ do not become zero in weak measurements, which may make relaxation dynamics under weak measurements distinct from those under projective measurements. Exploring the discrepancy and similarity between projective and weak measurements should be an interesting future work.

We thank Yohei Fuji and Hisanori Oshima for fruitful discussions, Nobuyuki Yoshioka and Toshihiro Yada for valuable comments on the manuscript, and Zongping Gong for both. Derivation of the spectral gap under no unitary gate given in Supplemental Material is partly based on a note written by Toshihiro Yada. This work was supported by JST ERATO Grant Number JPMJER2302, Japan. K.M. was supported by JSPS KAKENHI Grant. No. JP23K13037. R.H. was supported by JSPS KAKENHI Grant No. JP24K16982.

[1] S. Sachdev, *Quantum Phase Transitions* (Cambridge University Press, Cambridge, England, 2001).
 [2] M. B. Hastings and X.-G. Wen, Quasiadiabatic continuation of quantum states: The stability of topological ground-state degeneracy and emergent gauge invariance, *Phys. Rev. B* **72**, 045141 (2005).
 [3] E. M. Kessler, G. Giedke, A. Imamoglu, S. F. Yelin, M. D. Lukin, and J. I. Cirac, Dissipative phase transition in a central spin system, *Phys. Rev. A* **86**, 012116 (2012).

[4] Z. Cai and T. Barthel, Algebraic versus exponential decoherence in dissipative many-particle systems, *Phys. Rev. Lett.* **111**, 150403 (2013).
 [5] L. Bonnes, D. Charrier, and A. M. Läuchli, Dynamical and steady-state properties of a bose-hubbard chain with bond dissipation: A study based on matrix product operators, *Phys. Rev. A* **90**, 033612 (2014).
 [6] M. Žnidarič, Relaxation times of dissipative many-body quantum systems, *Phys. Rev. E* **92**, 042143 (2015).
 [7] F. Minganti, A. Biella, N. Bartolo, and C. Ciuti, Spectral theory of liouvillians for dissipative phase transitions, *Phys. Rev. A* **98**, 042118 (2018).
 [8] T. Mori and T. Shirai, Resolving a discrepancy between liouvillian gap and relaxation time in boundary-dissipated quantum many-body systems, *Phys. Rev. Lett.* **125**, 230604 (2020).
 [9] T. Haga, M. Nakagawa, R. Hamazaki, and M. Ueda, Liouvillian skin effect: Slowing down of relaxation processes without gap closing, *Phys. Rev. Lett.* **127**, 070402 (2021).
 [10] C. Holzhey, F. Larsen, and F. Wilczek, Geometric and renormalized entropy in conformal field theory, *Nuclear physics b* **424**, 443 (1994).
 [11] P. Calabrese and J. Cardy, Entanglement entropy and quantum field theory, *Journal of statistical mechanics: theory and experiment* **2004**, P06002 (2004).
 [12] M. B. Hastings and T. Koma, Spectral gap and exponential decay of correlations, *Communications in mathematical physics* **265**, 781 (2006).
 [13] M. B. Hastings, An area law for one-dimensional quantum systems, *Journal of statistical mechanics: theory and experiment* **2007**, P08024 (2007).
 [14] Y. Li, X. Chen, and M. P. A. Fisher, Quantum zeno effect and the many-body entanglement transition, *Phys. Rev. B* **98**, 205136 (2018).
 [15] X. Cao, A. Tilloy, and A. D. Luca, Entanglement in a fermion chain under continuous monitoring, *SciPost Phys.* **7**, 024 (2019).
 [16] A. Chan, R. M. Nandkishore, M. Pretko, and G. Smith, Unitary-projective entanglement dynamics, *Phys. Rev. B* **99**, 224307 (2019).
 [17] Y. Li, X. Chen, and M. P. A. Fisher, Measurement-driven entanglement transition in hybrid quantum circuits, *Phys. Rev. B* **100**, 134306 (2019).
 [18] B. Skinner, J. Ruhman, and A. Nahum, Measurement-induced phase transitions in the dynamics of entanglement, *Phys. Rev. X* **9**, 031009 (2019).
 [19] M. Szyniszewski, A. Romito, and H. Schomerus, Entanglement transition from variable-strength weak measurements, *Phys. Rev. B* **100**, 064204 (2019).
 [20] S. Choi, Y. Bao, X.-L. Qi, and E. Altman, Quantum error correction in scrambling dynamics and measurement-induced phase transition, *Phys. Rev. Lett.* **125**, 030505 (2020).
 [21] Y. Fuji and Y. Ashida, Measurement-induced quantum criticality under continuous monitoring, *Phys. Rev. B* **102**, 054302 (2020).
 [22] M. J. Gullans and D. A. Huse, Dynamical purification phase transition induced by quantum measurements, *Phys. Rev. X* **10**, 041020 (2020).
 [23] O. Lunt and A. Pal, Measurement-induced entanglement transitions in many-body localized systems, *Phys. Rev. Res.* **2**, 043072 (2020).
 [24] M. Szyniszewski, A. Romito, and H. Schomerus,

- Universality of entanglement transitions from stroboscopic to continuous measurements, *Phys. Rev. Lett.* **125**, 210602 (2020).
- [25] X. Turkeshi, R. Fazio, and M. Dalmonte, Measurement-induced criticality in $(2+1)$ -dimensional hybrid quantum circuits, *Phys. Rev. B* **102**, 014315 (2020).
- [26] O. Alberton, M. Buchhold, and S. Diehl, Entanglement transition in a monitored free-fermion chain: From extended criticality to area law, *Phys. Rev. Lett.* **126**, 170602 (2021).
- [27] T.-C. Lu and T. Grover, Spacetime duality between localization transitions and measurement-induced transitions, *PRX Quantum* **2**, 040319 (2021).
- [28] U. Agrawal, A. Zabalo, K. Chen, J. H. Wilson, A. C. Potter, J. H. Pixley, S. Gopalakrishnan, and R. Vasseur, Entanglement and charge-sharpening transitions in $u(1)$ symmetric monitored quantum circuits, *Phys. Rev. X* **12**, 041002 (2022).
- [29] F. Barratt, U. Agrawal, S. Gopalakrishnan, D. A. Huse, R. Vasseur, and A. C. Potter, Field theory of charge sharpening in symmetric monitored quantum circuits, *Phys. Rev. Lett.* **129**, 120604 (2022).
- [30] M. Block, Y. Bao, S. Choi, E. Altman, and N. Y. Yao, Measurement-induced transition in long-range interacting quantum circuits, *Phys. Rev. Lett.* **128**, 010604 (2022).
- [31] T. Minato, K. Sugimoto, T. Kuwahara, and K. Saito, Fate of measurement-induced phase transition in long-range interactions, *Phys. Rev. Lett.* **128**, 010603 (2022).
- [32] C. Noel, P. Niroula, D. Zhu, A. Risinger, L. Egan, D. Biswas, M. Cetina, A. V. Gorshkov, M. J. Gullans, D. A. Huse, and C. Monroe, Measurement-induced quantum phases realized in a trapped-ion quantum computer, *Nature Physics* **18**, 760 (2022).
- [33] P. Sierant and X. Turkeshi, Universal behavior beyond multifractality of wave functions at measurement-induced phase transitions, *Phys. Rev. Lett.* **128**, 130605 (2022).
- [34] A. Zabalo, M. J. Gullans, J. H. Wilson, R. Vasseur, A. W. W. Ludwig, S. Gopalakrishnan, D. A. Huse, and J. H. Pixley, Operator scaling dimensions and multifractality at measurement-induced transitions, *Phys. Rev. Lett.* **128**, 050602 (2022).
- [35] E. Granet, C. Zhang, and H. Dreyer, Volume-law to area-law entanglement transition in a nonunitary periodic gaussian circuit, *Phys. Rev. Lett.* **130**, 230401 (2023).
- [36] J. M. Koh, S.-N. Sun, M. Motta, and A. J. Minnich, Measurement-induced entanglement phase transition on a superconducting quantum processor with mid-circuit readout, *Nature Physics* **19**, 1314 (2023).
- [37] Y. Le Gal, X. Turkeshi, and M. Schirò, Volume-to-area law entanglement transition in a non-Hermitian free fermionic chain, *SciPost Physics* **14**, 138 (2023).
- [38] H. Lóio, A. De Luca, J. De Nardis, and X. Turkeshi, Purification timescales in monitored fermions, *Phys. Rev. B* **108**, L020306 (2023).
- [39] H. Oshima and Y. Fuji, Charge fluctuation and charge-resolved entanglement in a monitored quantum circuit with $u(1)$ symmetry, *Phys. Rev. B* **107**, 014308 (2023).
- [40] K. Yamamoto and R. Hamazaki, Localization properties in disordered quantum many-body dynamics under continuous measurement, *Phys. Rev. B* **107**, L220201 (2023).
- [41] A. Kumar, K. Aziz, A. Chakraborty, A. W. W. Ludwig, S. Gopalakrishnan, J. H. Pixley, and R. Vasseur, Boundary transfer matrix spectrum of measurement-induced transitions, *Phys. Rev. B* **109**, 014303 (2024).
- [42] K. Aziz, A. Chakraborty, and J. Pixley, Critical properties of weak measurement induced phase transitions in random quantum circuits, arXiv preprint arXiv:2404.02968 (2024).
- [43] K. Mochizuki and R. Hamazaki, Distinguishability transitions in nonunitary boson-sampling dynamics, *Phys. Rev. Res.* **5**, 013177 (2023).
- [44] See Supplemental Material for computation of the Lyapunov exponents, estimation of the spectral gap in the thermodynamic limit, derivation of the spectral gap when unitary gates are absent, and derivation of the upper bound for the width of the Lyapunov spectrum.
- [45] A. De Luca, C. Liu, A. Nahum, and T. Zhou, Universality classes for purification in nonunitary quantum processes, arXiv preprint arXiv:2312.17744 (2023).
- [46] V. B. Bulchandani, S. Sondhi, and J. Chalker, Random-matrix models of monitored quantum circuits, *Journal of Statistical Physics* **191**, 55 (2024).
- [47] B. Zeng, X. Chen, D.-L. Zhou, and X.-G. Wen, *Quantum information meets quantum matter* (Springer, 2019).
- [48] J. Eisert, M. Cramer, and M. B. Plenio, Colloquium: Area laws for the entanglement entropy, *Rev. Mod. Phys.* **82**, 277 (2010).
- [49] F. Hiai, Log-majorization and matrix norm inequalities with application to quantum information, arXiv preprint arXiv:2402.16067 (2024).

Supplemental Material for “Measurement-induced Spectral Transition”

Ken Mochizuki^{1,2} and Ryusuke Hamazaki^{2,3}

¹*Department of Applied Physics, University of Tokyo, Tokyo 113-8656, Japan*

²*Nonequilibrium Quantum Statistical Mechanics RIKEN Hakubi Research Team,*

RIKEN Cluster for Pioneering Research (CPR), 2-1 Hirosawa, Wako 351-0198, Saitama, Japan

³*RIKEN Interdisciplinary Theoretical and Mathematical Sciences*

Program (iTHEMS), 2-1 Hirosawa, Wako 351-0198, Saitama, Japan

S1. NUMERICAL PROCEDURE FOR COMPUTING LYAPUNOV EXPONENTS

We can compute the Lyapunov spectrum of noisy dynamics by focusing on time evolutions of state vectors [1], as considered in Refs. [2–5]. First, we choose n initial states $\{|\psi_0^i\rangle\}$ randomly, with $i = 1, 2, \dots, n$. We consider updating the state $|\phi_s^i\rangle = |\psi_{t=sb}^i\rangle$ by using the Gram-Schmidt orthonormalization procedure as follows:

$$|\varphi_{s+1}^i\rangle = \tilde{V}_{s,b} |\phi_s^i\rangle, \quad (\text{S1})$$

$$|\chi_{s+1}^i\rangle = (I_N - \Pi_{s+1}^i) |\varphi_{s+1}^i\rangle, \quad (\text{S2})$$

$$|\phi_{s+1}^i\rangle = |\chi_{s+1}^i\rangle / \sqrt{\langle \chi_{s+1}^i | \chi_{s+1}^i \rangle}, \quad (\text{S3})$$

where I_N is the $N \times N$ identity operator with $N = 2^L$ and $\tilde{V}_{s,b}$ is the time-evolution operator from $t = sb$ to $t = (s+1)b$ with s and b being integers. Here, $\Pi_s^i = \sum_{j=1}^{i-1} |\phi_s^j\rangle \langle \phi_s^j|$ with $i \geq 2$ is the projection operator onto the Hilbert space spanned by $\{|\phi_s^j\rangle\}_{j=1}^{i-1}$ and $\Pi_s^i = 0$ for $i = 1$.

Every time the dynamics proceed b steps, we compute Lyapunov exponents at $t = sb$ by evaluating decay rates of the evolution from $\{|\phi_s^i\rangle\}$ to $\{|\varphi_{s+1}^i\rangle\}$. At $t = sb$, the sum of the Lyapunov exponents $\tilde{\varepsilon}_{sb,i} = \sum_{j=1}^i \varepsilon_{sb,j}$ is obtained through

$$\tilde{\varepsilon}_{sb,i} = \frac{1}{sb} \sum_{r=1}^s \ln[\text{VOL}(\varphi_r^1, \varphi_r^2, \dots, \varphi_r^i)], \quad (\text{S4})$$

where $\text{VOL}(\varphi_r^1, \varphi_r^2, \dots, \varphi_r^i) = \sqrt{\det(\Phi_{r,i}^\dagger \Phi_{r,i})}$ is the volume of the space spanned by $\{|\varphi_r^j\rangle\}_{j=1}^i$, with $\Phi_{r,i} = (|\varphi_r^1\rangle, |\varphi_r^2\rangle, \dots, |\varphi_r^i\rangle)$. Then, $\tilde{\varepsilon}_i = \sum_{j=1}^i \varepsilon_j$ is defined as

$$\tilde{\varepsilon}_i = \lim_{s \rightarrow \infty} \tilde{\varepsilon}_{sb,i}. \quad (\text{S5})$$

We can easily obtain $\{\varepsilon_i\}$ and $\{\varepsilon_{t,i}\}$ from $\{\tilde{\varepsilon}_i\}$ and $\{\tilde{\varepsilon}_{t,i}\}$.

We apply the abovementioned method to our quantum dynamics exposed to the weak measurements. This is because computing Lyapunov exponents through the exact diagonalization of $V_t(\eta)V_t^\dagger(\eta)$ is difficult to carry out in the long-time regime, due to (i) the exponential decay of singular values $\{\Lambda_{t,i}(\eta)\}$, which makes $\{\Lambda_{t,i}(\eta)\}$ deviate from the numerical precision, and (ii) the longer computational time to diagonalize $V_t(\eta)$ whose matrix size is exponentially large with respect

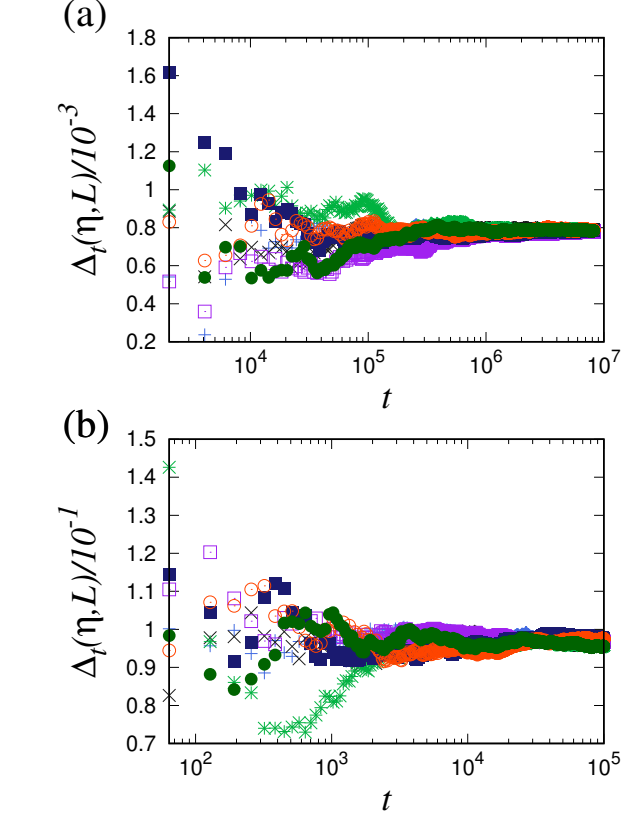


FIG. S1. Spectral gaps $\Delta_t(\eta, L)$ as functions of t with (a) $\eta = 0.1$ in the gapless phase and (b) $\eta = 0.3$ in the gapped phase. The different symbols correspond to different trajectories starting from randomly chosen initial states. The parameter b is taken to be $b = 2048$ in (a) and $b = 64$ in (b). The system size is $L = 12$ in both (a) and (b).

to L . The Kraus operators $\{M_t(\eta)\}$ included in $\tilde{V}_{s,b}(\eta) = M_{(s+1)b}(\eta)U_{(s+1)b}M_{(s+1)b-1}(\eta)U_{(s+1)b-1} \cdots M_{sb+1}(\eta)U_{sb+1}$, which are independent of i , are generated through the Born rule based on $|\psi_t^i(\eta)\rangle$. Figure S1 shows the spectral gap $\Delta_t(\eta)$ computed through various trajectories. We can understand that $\Delta_t(\eta)$ converge to a trajectory-independent value in both gapless and gapped phases. Likewise, we assume that $\varepsilon_{t,i}(\eta)$ converge to trajectory-independent values. Then, we compute the averages of $\{\varepsilon_{t,i}(\eta)\}$ over c steps from $t - bc$ to t through one

trajectory,

$$\langle \varepsilon_{t,i}(\eta) \rangle = \frac{1}{c} \sum_{\bar{c}=0}^{c-1} \varepsilon_{t-b\bar{c},i}(\eta), \quad (\text{S6})$$

where the value of c is taken in the range $100 \leq c \leq 1000$. When $\delta\varepsilon_{t,i}(\eta)/\langle \varepsilon_{t,i}(\eta) \rangle$ becomes smaller than some threshold d , we stop the numerical simulation and adopt the average as the i th Lyapunov exponent $\varepsilon_i(\eta) = \langle \varepsilon_{t,i}(\eta) \rangle$, where $\delta\varepsilon_{t,i}(\eta)$ is the standard deviation of $\varepsilon_{t,i}(\eta)$ with respect to time t . Here, we take d smaller than 3×10^{-2} .

We note that the numerical results depend on b when the value of b is too small. Thus, we explain how to choose b below. First, for the system size $L = 6 \times m_L$ and the error parameter $\eta = 0.1 \times m_\eta$, we compute $\Delta(\eta)$, where $m_L = 1, 2, 3$ and $m_\eta = 1, 2, 3, 4, 5, 6, 7$. Second, we increase b from some small value and compute the spectral gap for each b , with m_L, m_η , and c being fixed. If the Lyapunov exponents become independent of b for $b \geq b_{\min}(m_L, m_\eta, c)$ within the precision of $2d$, we use b larger than $b_{\min}(m_L, m_\eta, c)$ in the range $6 \times m_L \leq L < 6 \times (m_L + 1)$ and $0.1 \times (m_\eta - 1) < \eta \leq 0.1 \times m_\eta$.

Figure S2 shows the Lyapunov spectra up to $i = 10$ as functions of the system size L , obtained along the abovementioned scheme. Note that $\{\varepsilon_i(\eta, L)\}$ are shifted such that $\varepsilon_1(\eta, L) = 0$ is satisfied. The spectral gap $\Delta(\eta, L)$ with $\eta = 0.1$ exponentially decreases as L increases, while $\Delta(\eta, L)$ with $\eta = 0.7$ is almost independent of L . The low-lying excited spectrum $\{\varepsilon_i(\eta = 0.1)\}$ with $i \geq 2$ also exhibits the exponential decay with respect to L , which is different from that in the gapless phase of isolated quantum systems.

S2. EXTRAPOLATION OF THE SPECTRAL GAP

To obtain the spectral gap in the thermodynamic limit,

$$\Delta(\eta) = \lim_{L \rightarrow \infty} \Delta(\eta, L), \quad (\text{S7})$$

we extrapolate the numerical data $\Delta(\eta, L)$ in system sizes $10 \leq L \leq 22$. We use the least-squares method with the fitting function

$$\Delta_{\text{fit}}[C(\eta), L] = D(\eta) + a(\eta)[b(\eta)]^{-L}, \quad (\text{S8})$$

where $C(\eta) = [D(\eta), a(\eta), b(\eta)]$. Here, the function minimized is

$$\Theta[C(\eta)] = \sum_{L=10}^{22} \frac{(\Delta(\eta, L) - \Delta_{\text{fit}}[C(\eta), L])^2}{f^2(\eta, L)}, \quad (\text{S9})$$

where $f(\eta, L) = d \times \Delta(\eta, L)$. For each η , we adopt $\Delta(\eta)$ as the spectral gap in the thermodynamic limit, such that

$$\Theta[\Gamma(\eta)] = \min_{C(\eta)} \Theta[C(\eta)] \quad (\text{S10})$$

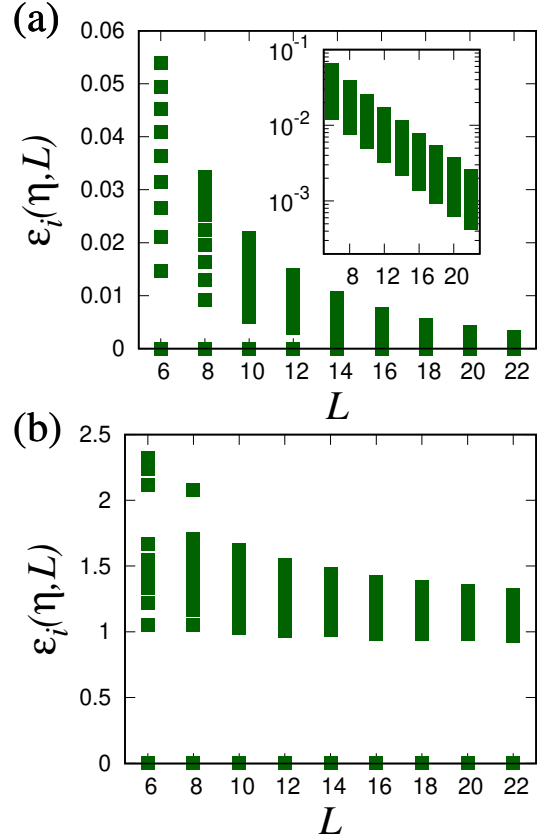


FIG. S2. Lyapunov spectra as functions of the system size L up to $i = 10$, with error parameters (a) $\eta = 0.1$ in the gapless phase and (b) $\eta = 0.7$ in the gapped phase. The inset in (a) is the semi-log plot of the data, showing that the low-lying Lyapunov spectrum exponentially decreases as L is increased.

is satisfied with $\Gamma(\eta) = [\Delta(\eta), \alpha(\eta), \beta(\eta)]$. For the minimization of $\Theta[C(\eta)]$, we explore the range of $D(\eta)$, from $-\min_L[\Delta(\eta, L)]$ to $+\min_L[\Delta(\eta, L)]$. Figure S3 shows the system-size dependence of the spectral gap, where the fitting curves $\Delta_{\text{fit}}[\Gamma(\eta), L]$ (blue broken line) and numerical data $\Delta(\eta, L)$ (green circles) agree well. As shown in Fig. S3, $\Delta(\eta, L)$ converges to $\Delta(\eta) \simeq 0$ for small η corresponding to the gapless phase, while $\Delta(\eta)$ is far from 0 for large η in the gapped phase.

After obtaining $\Delta(\eta)$, we compute the error bar of $\Delta(\eta)$ following the procedure explained below. We again sweep $D(\eta)$, $a(\eta)$, and $b(\eta)$ in the range $-\min_L[\Delta(\eta, L)] < D(\eta) < +\min_L[\Delta(\eta, L)]$, $0 < a(\eta) < 2\alpha(\eta)$, and $0 < b(\eta) < 2\beta(\eta)$, respectively. Then, we evaluate

$$\tilde{\Theta}[C(\eta)] = \sum_{L=10}^{22} \frac{(\Delta_{\text{fit}}[C(\eta), L] - \Delta_{\text{fit}}[\Gamma(\eta), L])^2}{f^2(\eta, L)}. \quad (\text{S11})$$

We obtain error bars of $\Delta(\eta)$ through $\min_{C(\eta)} D(\eta)$ and $\max_{C(\eta)} D(\eta)$ under the condition that $\tilde{\Theta}[C(\eta)] \leq \Theta[\Gamma(\eta)]$ is satisfied. Figure S4 shows $\Delta(\eta)$ and error bars obtained through the abovementioned method. We

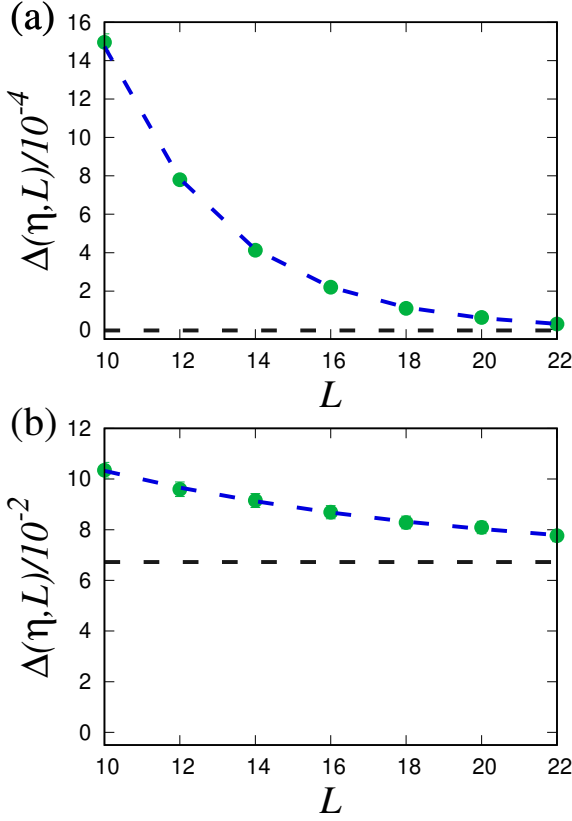


FIG. S3. The spectral gaps $\Delta(\eta, L)$ as functions of L , with (a) $\eta = 0.1$ in the gapless phase and (b) $\eta = 0.3$ in the gapped phase. The green circles are $\Delta(\eta, L)$, the blue broken lines represent the fitting curve $\Delta_{\text{fit}}[\Gamma(\eta), L]$, and the black broken lines are $\Delta(\eta)$. The fitting parameters are (a) $\Delta(\eta) \simeq -5.2 \times 10^{-6}$, $\alpha(\eta) \simeq 1.4$, $\beta(\eta) \simeq 3.4 \times 10^{-2}$ and (b) $\Delta(\eta) \simeq 6.7 \times 10^{-2}$, $\alpha(\eta) \simeq 1.1$, $\beta(\eta) \simeq 9.9 \times 10^{-2}$.

consider that the system with the error parameter η is in the gapless phase if $\min_{C(\eta)} D(\eta) < 0$ is satisfied, while $\min_{C(\eta)} D(\eta) > 0$ corresponds to the gapped phase. In the range $\eta < \eta_c = 0.2$, our numerical data satisfy the condition for the gapless phase.

S3. SPECTRAL GAP OF MEASUREMENT-ONLY DYNAMICS

Under some assumptions, we can analytically show that the spectral gap takes a non-zero value independent of the system size when unitary gates are absent. The final result is in Eq. (S29). In such a situation, all qubits are independent, and thus we can write $V_t(\eta)$ as

$$V_t(\eta) = \bigotimes_{\ell=1}^L V_{t,\ell}(\eta), \quad (\text{S12})$$

$$V_{t,\ell}(\eta) = \prod_{u=1}^t M_{\omega_{u,\ell}}(\eta), \quad (\text{S13})$$

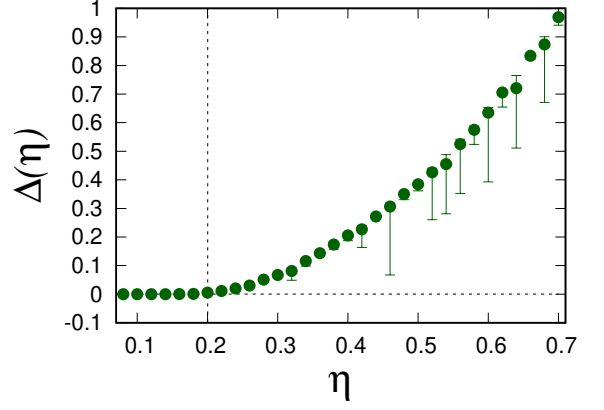


FIG. S4. The spectral gap $\Delta(\eta)$ as a function of η , which is obtained through the least-squares method.

where $V_{t,\ell}(\eta)$ is the 2×2 time-evolution operator for the site ℓ , and $\omega_{u,\ell} = \pm 1$ is probabilistically determined through the Born rule. The spectral gap and the Born probability are determined through the operators

$$M_+^\dagger(\eta)M_+(\eta) = \begin{pmatrix} p_\eta & 0 \\ 0 & 1-p_\eta \end{pmatrix}, \quad (\text{S14})$$

$$M_-^\dagger(\eta)M_-(\eta) = \begin{pmatrix} 1-p_\eta & 0 \\ 0 & p_\eta \end{pmatrix}, \quad (\text{S15})$$

where

$$p_\eta = \frac{(1+\eta)^2}{2(1+\eta^2)} \geq \frac{1}{2}. \quad (\text{S16})$$

In the following, we consider the case where $\eta \neq 0$ and thus $p_\eta \neq 1/2$ since $\eta = 0$ corresponds to no measurement. If $\omega_{u,\ell} = +1$ is realized v times from $u = 1$ to $u = t$ and $2v \geq t$, the singular values of $V_{t,\ell}(\eta)$ become

$$\Lambda_{t,\ell,v,1}(\eta) = \sqrt{p_\eta^v(1-p_\eta)^{t-v}}, \quad (\text{S17})$$

$$\Lambda_{t,\ell,v,2}(\eta) = \sqrt{p_\eta^{t-v}(1-p_\eta)^v}. \quad (\text{S18})$$

In this case, the spectral gap $\tilde{\Delta}_{t,\ell,v}(\eta)$ can be written as

$$\begin{aligned} \tilde{\Delta}_{t,\ell,v}(\eta) &= \left| \frac{1}{t} \ln \left[\frac{\Lambda_{t,\ell,v,1}(\eta)}{\Lambda_{t,\ell,v,2}(\eta)} \right] \right| \\ &= \frac{|t-2v|}{2t} \ln \left(\frac{p_\eta}{1-p_\eta} \right). \end{aligned} \quad (\text{S19})$$

We can easily check that the gap becomes the same even when $2v \leq t$.

Assuming a product initial state, $|\psi_0\rangle = \bigotimes_{\ell=1}^L |\psi_{0,\ell}\rangle$ with $|\psi_{0,\ell}\rangle = \begin{pmatrix} \psi_{0,\ell,\uparrow} \\ \psi_{0,\ell,\downarrow} \end{pmatrix}$, we find that the Born probability that $\omega_{u,\ell} = +1$ is realized v times becomes

$$\begin{aligned} &\langle \psi_{0,\ell} | V_{t,\ell}^\dagger(\eta) V_{t,\ell}(\eta) | \psi_{0,\ell} \rangle \\ &= \binom{t}{v} [p_\eta^v(1-p_\eta)^{t-v} |\psi_{0,\ell,\uparrow}|^2 + p_\eta^{t-v}(1-p_\eta)^v |\psi_{0,\ell,\downarrow}|^2]. \end{aligned} \quad (\text{S20})$$

Therefore, the ensemble average of the spectral gap at time step t can be written as

$$\langle \tilde{\Delta}_{t,\ell,v}(\eta) \rangle = \sum_{v=0}^t \binom{t}{v} p_\eta^v (1-p_\eta)^{t-v} \tilde{\Delta}_{t,\ell,v}(\eta) \quad (\text{S21})$$

Thus, the probability that the spectral gap is $\tilde{\Delta}_{t,\ell,v}(\eta)$ becomes the bimodal distribution. The mean value of v becomes $v_{t,\eta}^* = tp_\eta$, which leads to

$$\tilde{\Delta}_{t,\ell,v_{t,\eta}^*}(\eta) = \tilde{\Delta}^*(\eta) := \left(p_\eta - \frac{1}{2}\right) \ln \left(\frac{p_\eta}{1-p_\eta}\right). \quad (\text{S22})$$

When t is sufficiently large, we can show that almost all trajectories exhibit $\tilde{\Delta}_{t,\ell,v}(\eta) = \tilde{\Delta}^*(\eta)$. To this end, using $p_\eta > 1/2$ and thus $v_{t,\eta}^* > t/2$, we evaluate the probability that $|\tilde{\Delta}_{t,\ell,v}(\eta) - \tilde{\Delta}^*(\eta)| > \theta \ln \left(\frac{p_\eta}{1-p_\eta}\right)$ is satisfied,

$$\begin{aligned} & P \left[\left| \tilde{\Delta}_{t,\ell,v}(\eta) - \tilde{\Delta}^*(\eta) \right| > \theta \ln \left(\frac{p_\eta}{1-p_\eta} \right) \right] \\ &= P \left[\left| v - \frac{t}{2} \right| - \left| v_{t,\eta}^* - \frac{t}{2} \right| > t\theta \right] \\ &= P \left[|v - v_{t,\eta}^*| > t\theta, v > \frac{t}{2} \right] \\ &+ P \left[|t - (v + v_{t,\eta}^*)| > t\theta, v < \frac{t}{2} \right], \quad (\text{S23}) \end{aligned}$$

where θ is a positive value and $P \left[|v - v_{t,\eta}^*| > t\theta, v > \frac{t}{2} \right]$ is the joint probability that the conditions $|v - v_{t,\eta}^*| > t\theta$ and $v > \frac{t}{2}$ are satisfied. The probabilities in the right-hand side of Eq. (S23) satisfy

$$\begin{aligned} & P \left[|v - v_{t,\eta}^*| > t\theta, v > \frac{t}{2} \right] \\ &\leq P \left[|v_{t,\eta}^* - v| > t\theta \right], \quad (\text{S24}) \end{aligned}$$

$$\begin{aligned} & P \left[|t - (v + v_{t,\eta}^*)| > t\theta, v < \frac{t}{2} \right] \\ &\leq P \left[v < \frac{t}{2} \right] \leq P \left[|v_{t,\eta}^* - v| > v_{t,\eta}^* - \frac{t}{2} \right]. \quad (\text{S25}) \end{aligned}$$

Since the variance of the bimodal distribution becomes $\sigma_{t,\eta}^2 = tp_\eta(1-p_\eta)$, Eqs. (S23)-(S25) and the Chebyshev inequality lead to

$$\begin{aligned} & P \left[\left| \tilde{\Delta}_{t,\ell,v}(\eta) - \tilde{\Delta}^*(\eta) \right| > \theta \ln \left(\frac{p_\eta}{1-p_\eta} \right) \right] \\ &\leq \frac{p_\eta(1-p_\eta)}{t\theta^2} + \frac{p_\eta(1-p_\eta)}{t \left(p_\eta - \frac{1}{2}\right)^2}. \quad (\text{S26}) \end{aligned}$$

Through Eq. (S26), we can evaluate the probability that

$|\tilde{\Delta}_{t,\ell,v}(\eta) - \tilde{\Delta}^*(\eta)|$ becomes small at all sites ℓ :

$$\begin{aligned} & P \left[\left| \tilde{\Delta}_{t,\ell,v}(\eta) - \tilde{\Delta}^*(\eta) \right| \leq \theta \ln \left(\frac{p_\eta}{1-p_\eta} \right) \quad \forall \ell \right] \\ &= \prod_{\ell=1}^L \left(1 - P \left[\left| \tilde{\Delta}_{t,\ell,v}(\eta) - \tilde{\Delta}^*(\eta) \right| > \theta \ln \left(\frac{p_\eta}{1-p_\eta} \right) \right] \right) \\ &\geq \left[1 - \frac{p_\eta(1-p_\eta)}{t\theta^2} - \frac{p_\eta(1-p_\eta)}{t \left(p_\eta - \frac{1}{2}\right)^2} \right]^L \\ &\geq 1 - L \left[\frac{p_\eta(1-p_\eta)}{t\theta^2} + \frac{p_\eta(1-p_\eta)}{t \left(p_\eta - \frac{1}{2}\right)^2} \right]. \quad (\text{S27}) \end{aligned}$$

Therefore, if $t \gg Lp_\eta(1-p_\eta)/\theta^2$ and $t \gg Lp_\eta(1-p_\eta)/(p_\eta - \frac{1}{2})^2$ are satisfied, the spectral gap typically becomes $\tilde{\Delta}^*(\eta)$ for almost all trajectories. If we choose $\theta = O(1/L)$ and $t = \Omega(L^4)$ is satisfied, the probability that the gap satisfies $\tilde{\Delta}^*(\eta) - O(1/L) < \tilde{\Delta}_{t,\ell,v}(\eta) < \tilde{\Delta}^*(\eta) + O(1/L)$ for all ℓ becomes $1 - O(1/L)$. Then, for large t where $\tilde{\Delta}_{t,\ell,v}(\eta)$ has converged to $\tilde{\Delta}^*(\eta)$, the time-evolution operator becomes

$$V_{t,\ell}(\eta) \propto \begin{pmatrix} 1 & 0 \\ 0 & e^{-\Omega_{t,\ell} \tilde{\Delta}^*(\eta)t} \end{pmatrix}, \quad (\text{S28})$$

with $\Omega_{t,\ell} = \text{sign} \left(\sum_{u=1}^t \omega_{u,\ell} \right)$. In such a situation, through Eq. (S12), we can understand that the spectral gap of the whole system also becomes $\Delta(\eta) = \tilde{\Delta}^*(\eta)$:

$$\Delta(\eta) = \left(p_\eta - \frac{1}{2}\right) \ln \left(\frac{p_\eta}{1-p_\eta}\right). \quad (\text{S29})$$

Equation (S29) means that the system always resides in the gapped phase. In other words, the measurement-induced spectral transition revealed in the main text is caused by the competition between unitary dynamics and quantum measurements.

S4. EVALUATION OF THE SPECTRAL WIDTH BASED ON THE MAJORIZATION

To evaluate the maximal width of the Lyapunov spectrum, we consider the majorization for arrays of real numbers $u = (u_1, u_2, \dots, u_N)$, where $u_i \geq u_{i+1}$ is satisfied. The majorization of two arrays u and v ,

$$u \prec v, \quad (\text{S30})$$

is defined as

$$\sum_{i=1}^n u_i \leq \sum_{i=1}^n v_i, \quad (\text{S31})$$

where the equality is achieved for $n = N$. If u and v satisfy $u \prec v$, there exists a doubly stochastic matrix W , which satisfies

$$u = Wv. \quad (\text{S32})$$

Here, a doubly stochastic matrix is defined as a non-negative matrix satisfying $\sum_i W_{ij} = \sum_i W_{ji} = 1$ for arbitrary j .

The log-majorization of two arrays u and v ,

$$u \prec_{\log} v, \quad (\text{S33})$$

is defined as

$$\prod_{i=1}^n u_i \leq \prod_{i=1}^n v_i, \quad (\text{S34})$$

where the equality is satisfied for $n = N$. We consider the log-majorization for the singular values of matrices. Given a matrix A , we consider the array $s(A) = [s_1(A), s_2(A), \dots, s_N(A)]$, where $\{s_i(A)\}$ denote the singular values of A and $s_i(A) \geq s_{i+1}(A)$ is satisfied. The Horn theorem tells us that a product of two matrices satisfies

$$s(AB) \prec_{\log} s(A)s(B), \quad (\text{S35})$$

where $s(A)s(B) = [s_1(A)s_1(B), \dots, s_N(A)s_N(B)]$ [6].

We apply the properties of the majorizations explained above to our Kraus operators. From Eq. (S35), we can show that each Kraus operator satisfies

$$s[M_t(\eta)] \prec_{\log} s[\tilde{M}_{\omega_t, \ell=1}(\eta)] s[\tilde{M}_{\omega_t, \ell=2}(\eta)] \cdots s[\tilde{M}_{\omega_t, \ell=L}(\eta)] = \mathbb{M}(\eta), \quad (\text{S36})$$

where $\tilde{M}_{\omega_t, \ell}(\eta) = \left[\bigotimes_{m=1}^{\ell-1} \sigma_0 \right] \otimes M_{\omega_t, \ell}(\eta) \otimes \left[\bigotimes_{m=\ell+1}^L \sigma_0 \right]$ with σ_0 being the 2×2 identity matrix. Here, the array $\mathbb{M}(\eta)$ is independent of $\{\omega_{t, \ell}\}$,

$$[\mathbb{M}(\eta)]_i = \begin{cases} \left[\frac{1+\eta}{\sqrt{2(1+\eta^2)}} \right]^L & (1 \leq i \leq N/2), \\ \left[\frac{1-\eta}{\sqrt{2(1+\eta^2)}} \right]^L & (N/2 < i \leq N), \end{cases} \quad (\text{S37})$$

where $N = 2^L$. This is because singular values of $M_+(\eta)$ and $M_-(\eta)$ are the same, $[(1+\eta)/\sqrt{2(1+\eta^2)}, (1-\eta)/\sqrt{2(1+\eta^2)}]$. In a similar manner, from Eqs. (S35)

and (S36), we can understand that our time-evolution operator $V_t(\eta) = M_t(\eta)U_t \cdots M_1(\eta)U_1$ satisfies

$$s[V_t(\eta)] \prec_{\log} s[M_1(\eta)] \cdots s[M_t(\eta)] \prec_{\log} \mathbb{M}_t(\eta), \quad (\text{S38})$$

where the array $\mathbb{M}_t(\eta)$, which is independent of measurement outcomes, is

$$[\mathbb{M}_t(\eta)]_i = \begin{cases} \left[\frac{1+\eta}{\sqrt{2(1+\eta^2)}} \right]^{Lt} & (1 \leq i \leq N/2), \\ \left[\frac{1-\eta}{\sqrt{2(1+\eta^2)}} \right]^{Lt} & (N/2 < i \leq N). \end{cases} \quad (\text{S39})$$

Note that the right-hand side of Eq. (S38) is independent of unitary matrices $\{U_t\}$ because of $s_i(U_t) = 1$. Equation (S38) means that an array

$$\mu_i(\eta, L) = \begin{cases} L \ln \left[\frac{1+\eta}{\sqrt{2(1+\eta^2)}} \right] & (1 \leq i \leq N/2), \\ L \ln \left[\frac{1-\eta}{\sqrt{2(1+\eta^2)}} \right] & (N/2 < i \leq N) \end{cases} \quad (\text{S40})$$

majorizes $-\varepsilon(\eta, L)$,

$$-\varepsilon(\eta, L) \prec \mu(\eta, L), \quad (\text{S41})$$

where $-\varepsilon(\eta, L) = [-\varepsilon_1(\eta, L), \dots, -\varepsilon_N(\eta, L)]$. This means that $-\varepsilon(\eta, L)$ and $\mu(\eta, L)$ are related by a doubly stochastic matrix $W(\eta, L)$, that is,

$$\varepsilon_i(\eta, L) = L \left(w_i(\eta, L) \ln \left[\frac{\sqrt{2(1+\eta^2)}}{1+\eta} \right] + [1 - w_i(\eta, L)] \ln \left[\frac{\sqrt{2(1+\eta^2)}}{1-\eta} \right] \right) \quad (\text{S42})$$

is satisfied with $w_i(\eta, L) = \sum_{j=1}^{N/2} W_{ij}(\eta, L)$ being real and non-negative numbers less than 1. This results in

$$\begin{aligned} \varepsilon_N(\eta, L) - \varepsilon_1(\eta, L) &= L[w_1(\eta, L) - w_N(\eta, L)] \ln \left(\frac{1+\eta}{1-\eta} \right). \end{aligned} \quad (\text{S43})$$

Since the coefficients reside in the range $0 \leq w_i(\eta, L) \leq 1$, the upper bound of the spectral width becomes $O(L)$,

$$\varepsilon_N(\eta, L) - \varepsilon_1(\eta, L) \leq L \ln \left(\frac{1+\eta}{1-\eta} \right). \quad (\text{S44})$$

Thus, the typical level spacing becomes $O(e^{-L})$ since the number of $\{\varepsilon_i(\eta)\}$ is $N = 2^L$.

[1] A. Crisanti, G. Paladin, and A. Vulpiani, Products of random matrices in Statistical Physics, Vol. 104 (Springer Science & Business Media, 2012).

[2] A. Zabalo, M. J. Gullans, J. H. Wilson, R. Vasseur, A. W. W. Ludwig, S. Gopalakrishnan, D. A. Huse, and J. H. Pixley, Operator scaling dimensions and

- multifractality at measurement-induced transitions, Phys. Rev. Lett. **128**, 050602 (2022).
- [3] A. Kumar, K. Aziz, A. Chakraborty, A. W. W. Ludwig, S. Gopalakrishnan, J. H. Pixley, and R. Vasseur, Boundary transfer matrix spectrum of measurement-induced transitions, Phys. Rev. B **109**, 014303 (2024).
- [4] K. Mochizuki and R. Hamazaki, Absorption to fluctuating bunching states in nonunitary boson dynamics, Phys. Rev. Res. **6**, 013004 (2024).
- [5] K. Aziz, A. Chakraborty, and J. Pixley, Critical properties of weak measurement induced phase transitions in random quantum circuits, arXiv preprint arXiv:2404.02968 (2024).
- [6] F. Hiai, Log-majorization and matrix norm inequalities with application to quantum information, arXiv preprint arXiv:2402.16067 (2024).